Improved Non-Pt Alloys for the Oxygen Reduction Reaction at Fuel Cell Cathodes Predicted from Quantum Mechanics

Ted H. Yu, Yao Sha, Boris V. Merinov,* and William A. Goddard III*

Materials and Process Simulation Center (139-74), California Institute of Technology, Pasadena, California 91125

Received: March 18, 2010; Revised Manuscript Received: May 14, 2010

Based on studies on Pt_3Co and Pt_3Ni, we developed the hypothesis that improved alloy catalysts for the oxygen reduction reaction (ORR) at fuel cell cathodes should have a surface layer that is noble (e.g., Pt, Pd, or Rh) while the second layer should have ~50% electropositive metal to decrease the critical barriers for ORR, and we used quantum mechanics (QM) to examine 80 binary alloys of composition Y_3X, where Y = Pt, Pd, Rh, and X is any of the three rows of transition metals (columns 3−11). This study identified that for Pd_3X, good segregating alloys include X = Re (best), W, Os, Mo, Ru, Ir, Tc, Rh, Co, Ta, Nb, and Ni. Of these we selected Pd_3W as particularly promising since it is known experimentally to form an ordered alloy and was found to have a desirable d-band center. We then examined the critical barriers for various steps of the ORR with Pd_3W and compared them to the analogous barriers for Pt, Pt_3Co, and Pd. These results suggest that Pd_3W will exhibit ORR properties dramatically improved over pure Pd and close to that of pure Pt. The cost of Pd_3W is ~6 times less than pure Pt, suggesting that Pd_3W catalysts might lead to significant decreases in catalyst cost, while maintaining performance.

Introduction

The major motivation for this study is to find dramatically less expensive cathode catalysts for polymer electrolyte membrane fuel cell (PEMFC) than pure Pt, while maintaining or improving the high performance for the oxygen reduction reaction (ORR) exhibited by Pt. An obvious candidate would be to replace Pt by Pd, which would decrease the cost by a factor of 5.[1] However, the performance of Pd for ORR is dramatically worse[2] than that for Pt. Thus we explored other possible alloys[3,4] of Pd that might lead to higher performance. Here we were stimulated by the observation that Pt_3Co and Pt_3Ni have enhanced ORR catalytic activity over pure Pt[5,6] and also lead to a unique segregation in which the first layer is 100% Pt while the second layer is ~50% in the base metal[7,8] Co or Ni. We found from QM calculations that although the second layer is completely covered by the surface layer, the 50% concentration of Ni or Co in the second layer enhances the ORR of the surface layer (pure Pt), while the noble metal overlayer helps protect the electropositive metal from oxidation. Even so the Co and Ni alloying elements tend to become depleted from the surface under FC operating conditions.[9]

To determine new alloy candidates for PEMFC cathodes, we considered 80 binary alloys of composition Y_3X, where Y = Pt, Pd, Rh, and X is any of the three rows of transition metals (columns 3−12). Our strategy was first to find all binary alloys in which there is a strong segregation of the noble metal to the surface (100%) with a concomitant enrichment of the base metal in the second layer (50%).[10−13] Here we used QM calculations [density functional theory (DFT) of the PBE[14] flavor] on a 4 layer slab to determine these energy differences. These studies correctly identified that Pt_3Co (0.50 eV) and Pt_3Ni (0.46 eV) would have this segregation property while Pt_3Fe (0.11 eV) would not, as observed from LEED experiments.[7] Of these systems with a strong preference for segregation, we selected the ones known to have a Y_3X intermetallic phase as most likely to lead to a stable noble metal protecting surface. This led to identifying Pd_3W as particularly promising.

Having selected the systems with the best surface segregation, we then used QM to examine the reaction pathways for ORR, comparing Pd_3W with bulk Pd and bulk Pt and also with Pt_3Co. We find that Pt_3Co is better than Pt, as observed, and that Pd is much worse than Pt, as observed. We find that Pd_3W has a performance much better than Pd, suggesting that it is an excellent candidate for experimental study.

Computational Methods

Periodic quantum mechanics (QM) calculations were carried out with the SeqQuest code,[15,16] which employs Gaussian basis functions rather than the plane wave basis often used in periodic systems. We used the Perdew−Becke−Ernzerhof (PBE) flavor[14] of DFT in the generalized gradient approximation (GGA)[17,18] and allowed the up-spin orbitals to be optimized independently of the down-spin orbitals (spin unrestricted DFT). All calculations were performed with spin optimization.

Angular-momentum-projected norm-conserving nonlocal effective core potentials[19−22] (pseudopotentials) were used to replace the core electrons. Thus, the Pt atom was described with 16 explicit electrons (six 5p, one 6s, and nine 5d in the ground state). The Gaussian basis functions were contracted to the double-ζ plus polarization level from calculations on the most stable unit cell of the pure elements. The real space grid density was 5 points per angstrom, while the reciprocal space grid was $5 \times 5 \times 0$ for slab calculations.

For the three-dimensional structure we assumed the $L1_2$ cubic unit cell with the base metal X at the corner and the noble metal Y centered on the faces, and then we optimized the lattice parameter [tabulated in the Supporting Information, Table S1]. The reciprocal space grid was $12 \times 12 \times 12$. The bulk spin is tabulated in Table S3 (Supporting Information).

* To whom correspondence should be addressed. E-mail: merinov@wag.caltech.edu (B.V.M.) and wag@wag.caltech.edu (W.A.G.).

10.1021/jp1024735
Published on Web 06/10/2010

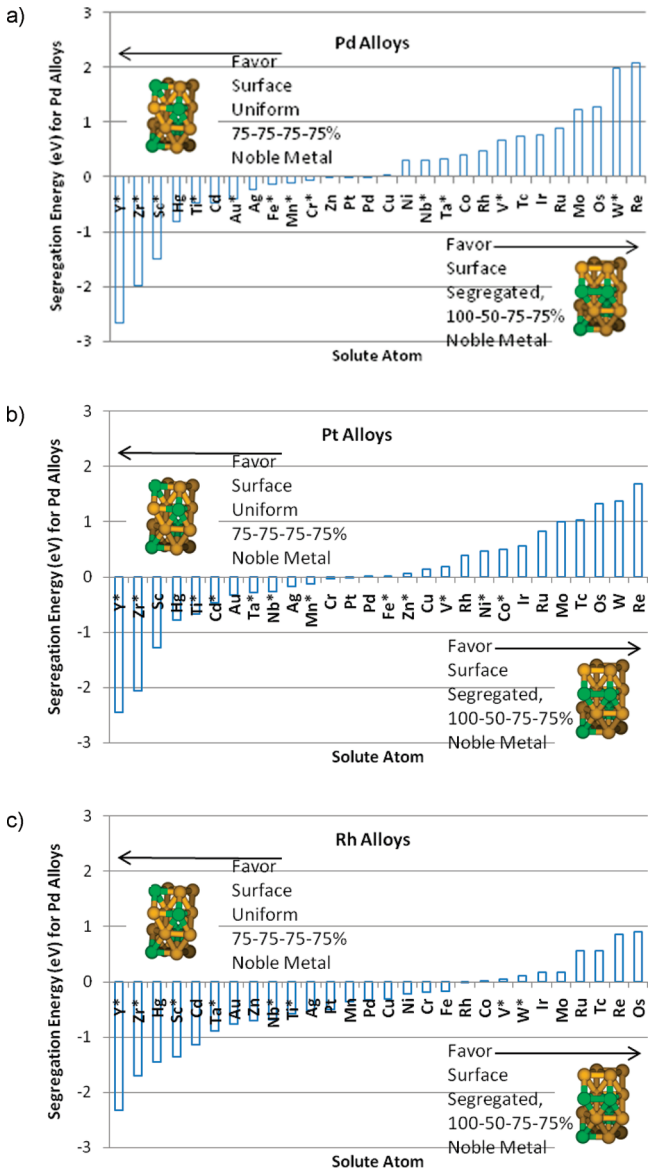

Figure 1. Illustration of the structures used for predicting segregation of Y_3X alloys. We use a two dimensionally infinite four-layer (bottom layer fixed) slab of closest packed atoms with 4 independent atoms per layer. Here the 4 base metals, X, are shown in green, while the 12 noble metal atoms, Y, are gold. Shown is the segregation energy of (a) Pd_3X, (b) Pt_3X, and (c) Rh_3X alloys, where positive implies segregation with the top layer pure Y, and the second layer 50% Y. An asterisk (*) next to the base metal indicates a stable Y_3X phase has been observed experimentally.

To describe the surface segregation and ORR, we assumed the closest packed (111) and used the 2×2 hexagonal periodic unit cell in the *a* and *b* directions based on the bulk lattice constants, while allowing 4 independent metal atoms for each of the 4 layers. For calculating segregation energies, we considered the four-layer slab (Figure 1), in which the top two layers are allowed to relax, but the bottom two layers were fixed with the atoms in their bulk structure positions. The spin of the four-layer slabs is tabulated in Table S3 (Supporting Information). The five- and six-layer slabs were also calculated for some cases with the top two layers relaxed and the remaining layers fixed. The segregation energy was found to be comparable for the four-, five-, and six-layer cases, indicating that the four-layer case is sufficient (tabulated in the Supporting Information, Table S2). A vertical mirror symmetry plane was added perpendicular to the layers in all cases. We also calculated electron density of states (using SeqQuest)[23] to obtain the surface d-band center of the alloys.

To calculate the energetics of second layer enrichment of 3-d base atoms, we used 2×2 five-layer slabs (Figure 3) with the third layer fixed. Here the lattice parameter was taken as the average lattice parameter of the two alloys being compared. For example, to compare Pt_3Co and Pt_3Fe, we used the average of the calculated FCC lattice parameter of the two. Similar to the 4-layer slabs, a vertical mirror plane was added perpendicular to the layers.

To calculate the reaction pathway and barrier for the various ORR reactions, we used a three-layer slab, in which the top two layers were allowed to relax but the bottom layer was fixed. Due to the use of Gaussian basis functions, it was not necessary to add an artificial vacuum surface as is often done with plane wave basis sets.[24]

Water plays an important role in PEMFCs, being present in the PEM, fuel, and oxidant. Thus solvation by the water must be included to obtain the energetics and rates relevant for ORR. To estimate this solvent effect, we used the Poisson−Boltzmann model as implemented in the Adaptive Poisson−Boltzmann Solver (APBS),[25,26] which we adapted to periodic boundary conditions and SeqQuest (we took the dielectric constant as 78 and the solvent radius as 1.4 Å). These calculations were carried out with the CMDF[27] module to obtain the free energy reaction surface for the ORR.

Results and Discussion

Segregation. Table 1 reports the segregation energies calculated for Pd_3X, Pt_3X, and Rh_3X, comparing surface segregated (pure noble metal, Y, in the top layer, 50% of X in the second layer, and 25% in subsequent layers) and surface uniform (a uniform distribution of 25% X in every layer). A positive value indicates that segregation is favorable. Figure 1a−c shows this graphically.

Validations of our calculations can be made by comparing with experimental segregation results. Pd−Co,[28] Pd−Ni,[29] Pt−Fe,[7,8,30] Pt−Co,[7,31] Pt−Ni,[7,32] Pt−Cu,[33] Pt−Ir,[34] Pt−Ru,[35,36] Pt−Mo,[37] and Pt−Rh[7,36,38] alloys have been shown to have Pt segregated to the surface, with the percent of Pt higher than that of the bulk concentration, corresponding to the positive segregation energy calculated in this study. In addition to the top layer being enriched in noble metal, Pd−Ni,[29] Pt−Co,[7] Pt−Ni, Pt−Cu,[33] Pt−Rh,[36,38] and Pt−Ru[36] were shown experimentally to have second layer enrichment of base metal by low energy electron diffraction (LEED), medium energy ion scattering (MEIS), or depth profiling, also corresponding to a positive segregation energy. A useful technique for surface characterization of Pt_3Co, Pt_3Ni, and Pt_3Fe is low energy ion scattering (LEIS),[30,39] which is capable of determining quantitatively the composition of the surface layer. However, LEIS is not sensitive to the second layer elements and will not detect second layer enrichment of base metals, which can be detected with LEED and MEIS. In our calculations, negative segregation energy implies segregation of the base metal to the surface. Experiments have been conducted on Pd−Au,[39] Pd−Ag,[39,40] and Pt−Au[41,42] that show segregation of the base metal to the surface corresponding to the negative segregation energy calculated in this study.

Further validation of our calculations is given in Figure 2, where we compare the theoretical segregation energy of Pt_3Fe, Pt_3Co, and Pt_3Ni with the degree of surface segregation found in low-energy electron diffraction (LEED) experiment by Gauthier.[7] For Pt_3Co and Pt_3Ni, LEED experiments show that

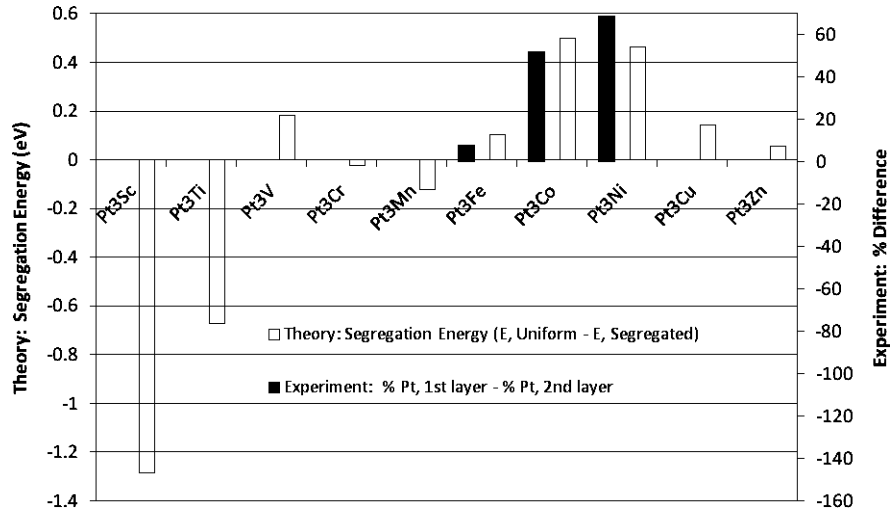

Figure 2. Predicted segregation energies from theory for Pt_3X alloys, where positive shows that 100% Pt is preferred in the top layer and 50% in the second layer. Experimental results are the following: Pt_3Co: 100% Pt in the top layer and 48% in the second layer (52% difference); Pt_3Ni: 99% Pt in the top layer and 30% in the second layer (69% difference); Pt_3Fe: 96% Pt in the top layer and 88% in the second layer (8% difference). Here we have plotted the difference between the experimental top and second layer Pt concentrations.

TABLE 1: Segregation Energy (eV) of Various Y_3X Metal Alloys, Where Y = Pd, Pt, Rh, and X Is a Transition Metal[a]

	base				base		
noble	Pd	Pt	Rh	noble	Pd	Pt	Rh
Y	–2.679*	–2.451*	–2.326*	Cu	0.031	0.142	–0.307
Zr	–1.983*	–2.062*	–1.708*	Ni	0.311	0.462*	–0.217
Sc	–1.496*	–1.286	–1.356*	Nb	0.311*	–0.266*	–0.692*
Hg	–0.822	–0.778	–1.451	Ta	0.334*	–0.281*	–0.891*
Ti	–0.477*	–0.671*	–0.572*	Co	0.409	0.500*	0.007
Cd	–0.471	–0.468*	–1.133	Rh	0.474	0.391	0.000
Au	–0.392*	–0.328	–0.757	Tc	0.742	1.029	0.555
Ag	–0.223	–0.177	–0.513	V	0.668*	0.181*	0.054*
Fe	–0.133*	0.105*	–0.170	Ir	0.764	0.566	0.175
Mn	–0.105*	–0.122*	–0.358	Ru	0.884	0.830	0.555
Cr	–0.074*	–0.023	–0.189	Mo	1.232	1.002	0.178
Zn	–0.001	0.056*	–0.705	Os	1.275	1.327	0.909
Pt	–0.001	0.000	–0.501	W	1.996*	1.372	0.108*
Pd	0.000	0.005	–0.335	Re	2.089	1.686	0.853

[a] Large positive segregation energy implies that the top layer is pure noble metal, while the second layer is 50% noble metal. An asterisk (*) next to the segregation energy indicates that a Y_3X phase has been observed experimentally. X is ordered by the segregation energy for Pd_3X.

the surface layer concentration is nearly 100% Pt, while the second layer is about 50% Co or Ni, and the third is nearly 75% Pt. Consistent with this the theory predicts that this segregated structure is more stable than the uniform by 0.50 eV for X = Co and 0.46 eV for X = Ni. In contrast the LEED shows very little second layer Fe enrichment in Pt_3Fe, which is consistent with the much smaller segregation energies (0.10 eV) predicted for Fe and other 3d metals.

A comprehensive early study[11] of surface segregation energies assuming 1 × 1 surfaces considered nearly all combinations of bimetallic transition metal alloys. However, our systematic studies used 2 × 2 layers allowing comparison of layers with mixed concentration per layer (0%, 25%, 50%, 75%, 100%), whereas the 1 × 1 comparison study can only compare 0% or 100%. A similar study with five 2 × 2 layers for surface structures of Pt_3X alloys (but not Rh_3X and Pd_3X alloys) comparing "surface segregated" and "surface uniform" cases[13] has similar qualitative results for the Pt alloy cases in this study (all segregation energies have the same signs). Quantitatively, the one case where the results differ significantly is for Pt_3Fe where ref 13 shows segregation energy of 0.41 eV (ref 13 displays the energy as −0.41 rather than +0.41). In contrast we considered the four, five, and six layers (see Tables 1, 2 and in the Supporting Information Table S2) all of which show small positive segregation energy in Pt_3Fe (0.10−0.12 eV). Otherwise, the Pt results in this study are consistent with the results with Balbuena[13] leading to a mean average difference of 0.097 eV. Other than the cases when the segregation energies are very large (Pt_3Re and Pt_3Mo) and the Pt_3Fe case, the values compare well and are within 0.15 eV difference.

The reason for the difference in Pt_3Fe segregation energy between this study and Balbuena's[13] must be due to small differences in the DFT calculation. Both studies use the PBE[14] flavor of DFT, but one potentially important difference is in the core effective potentials (pseudopotentials). We treat 16 valence electrons for Pt and 14 valence electrons for Fe, while VASP uses 10 valence electrons for Pt and 8 valence electrons for Fe. We expect that explicitly describing the occupied 3p electrons is essential to an accurate description for Fe, Co, and Ni due to the very small size of the 3d electrons. A second difference is that we use Gaussian basis sets (rather than plane wave basis sets), which allow us to validate against very accurate slab calculations.

Figure 1a−c identifies even more strongly segregating base atoms for Pt, including Re (best), W, Os, Tc, Mo, Ru, Ir (in decreasing segregation energy). More importantly we identified a number of base atom cases for Pd favoring a strong tendency for segregation: Re (best), W, Os, Mo, Ru, Ir, Tc, Rh, Co, Ta, Nb, and Ni in decreasing segregation energy (Table 1 and Figure 1). In general, the segregation energies of Pd and Pt alloys are similar for the same base atoms. But in all cases, Rh alloys lead to lower segregation energies than Pd and Pt alloy for the same base metal. The best base atoms for high segregation energy are metals with high cohesive energy, such as Re, W, Os, and Mo.

Among the Pd_3X alloys with strong segregation energies, only Pd_3W is known to have a stable phase at this 3:1 composition,[43,44] as also observed for Pt_3Co and Pt_3Ni alloys. We expect that such systems with a stable ordered phase at 3:1 ratio are more likely to be ordered. This, plus the relative abundance of W, makes Pd_3W a most promising candidate for investigating the catalytic properties. In addition, we consider Pd_3Ta, Pd_3V, and

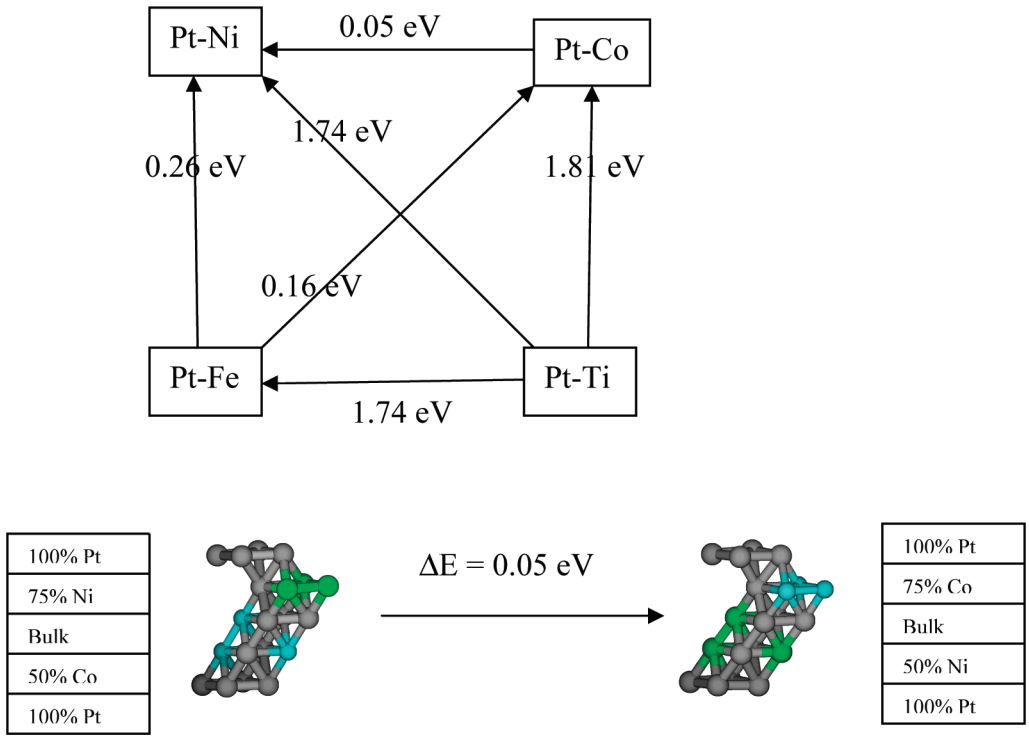

Figure 3. Predicted second layer base metal enrichment energies of Pt_3Co, Pt_3Ni, Pt_3Fe, and Pt_3Ti. The diagram compares the energetics of second layer base metal enrichment between alloys. Pt_3Ni was found to be slightly more favored to be enriched than Pt_3Co by 0.05 eV. Of the alloys, Pt_3Ti was found to be least likely to be enriched by ~1.7 eV versus the other alloys. This figure explains why these alloys have been experimentally found to be nearly 100% Pt on the surface layer, while their calculated segregation energy varied significantly. The difference in segregation energy is due to the difference in the second layer enrichment energies.

TABLE 2: d-Band Center (eV) of Various Y_3X Metal Alloys, Where Y = Pd, Pt, Rh, and X Is a Transition Metal[a]

	base				base		
noble	Pd	Pt	Rh	noble	Pd	Pt	Rh
Ta	–2.44	–2.85	–2.13	Co	–2.08	–2.75	–2.17
W	–2.39	–2.95	–2.27	Ir	–2.03	–2.65	–2.24
Ti	–2.37	–2.78	–2.10	Ni	–2.03	–2.70	–2.19
Nb	–2.37	–2.79	–2.10	Mn	–1.98	–2.65	–2.16
V	–2.31	–2.84	–2.26	Y	–1.97	–2.23	–1.59
Re	–2.28	–2.85	–2.31	Rh	–1.95	–2.59	–2.16
Zr	–2.25	–2.55	–1.86	Cu	–1.92	–2.58	–2.11
Mo	–2.25	–2.83	–2.26	Zn	–1.89	–2.58	–1.91
Os	–2.21	–2.76	–2.27	Pt	–1.83	–2.47	–2.09
Tc	–2.21	–2.79	–2.29	Pd	–1.82	–2.44	–2.04
Sc	–2.12	–2.52	–1.77	Cd	–1.66	–2.24	–1.70
Cr	–2.11	–2.73	–2.26	Au	–1.61	–2.18	–1.88
Ru	–2.11	–2.68	–2.23	Ag	–1.59	–2.17	–1.85
Fe	–2.10	–2.71	–2.10	Hg	–1.57	–2.13	–1.69

[a] We see that Pd_3Ta and Pd_3W are most negative and closest to Pt.

Pd_3Nb with their moderately positive segregation energy (comparable to Pt_3Co and Pt_3Ni) and stable 3:1 phase as other good candidates.[43,45]

Second Layer Enrichment of Base Metal. Figure 3 compares calculations of the second layer enrichment of base metals in a 3:1 alloy. Because the segregation energy calculated in the previous section is a measure of both the tendency for an alloy to have 100% noble metal at the surface and enrichment of 50% base metal at the second layer, we perform energy calculations that measure only the second layer effects. We are motivated by the experimental findings that Pt_3Ni, Pt_3Co, Pt_3Fe, and Pt_3Ti have nearly 100% Pt[7,8,30−32,46] on the surface, while the theoretical segregation energy varies dramatically (0.46, 0.50, 0.11, and −0.67 eV, respectively). The five-layer cells for the calculations and the energetic results are shown in Figure 3, where we find that in terms of second layer enrichment of base metals the order is as follows: $Pt_3Ni > Pt_3Co > Pt_3Fe > Pt_3Ti$. Pt_3Ti has a very large energetic penalty to be enriched in Ti in the second layer of 1.7−1.8 eV compared to Pt_3Fe, Pt_3Co, and Pt_3Ni. This explains why the segregation energy of Pt_3Ti is negative (−0.67), even though experiments[46] show that the surface of Pt_3Ti is nearly 100% Pt (described in previous theory[13]). Pt_3Fe has a moderate second layer base metal enrichment penalty compared with Pt_3Co and Pt_3Ni (0.16 and 0.26 eV, respectively), which is consistent with experiment[7] and theory (see Figure 2). The experimental second layer concentration of Pt in Pt_3Fe, Pt_3Co, and Pt_3Ni is 88%, 48%, and 30% Pt, respectively. As such, Pt_3Fe has a second layer that is depleted in base metal (12% Fe < 25% Fe in bulk), whereas both Pt_3Co and Pt_3Ni are enriched in base metal. In summary, the segregation energy of alloys, that experiments have shown to be nearly 100% Pt at the surface, differ because of the energetic penalties associated with having 50% base metal in the second layer.

d-Band Centers of Alloys. For alloy catalysts, Norskov proposed a simple model that correlates the d-band center of the surface metal to catalytic activity.[47] Indeed, the adsorption energy of simple adsorbates (O, CO, H) was found to correlate well with the center of the surface metal d-band.[47,48] We report the d-band center of the surface layer of the surface segregated (100%−50%−75%−75% noble metal) case in Table 2. We see that the most negative d-band shifting base atom for Pd is Ta (−2.44 eV) followed by W (−2.39 eV), making them the non-Pt alloys with d-bands closest to Pt. The d-band centers of Rh alloys are more positive than both Pd and Pt alloys. In comparison, the d-band centers for notable catalysts include pure Pt (−2.47 eV), Pt_3Co (−2.75), and Pt_3Ni (−2.70). Thus, the

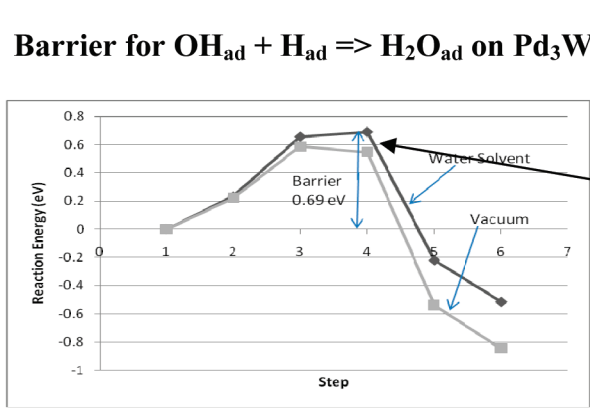

Barrier in water (eV)	Pd	Pd_3W	Pt	Pt_3Co
i) $O_{2ad} => 2O_{ad}$	**0.18**	**0.57**	0.00	1.05
ii) $O_{ad} + H_{ad} => OH_{ad}$	**0.41**	**0.26**	1.23	0.62
iii) $OH_{ad} + H_{ad} => H_2O_{ad}$	**0.76**	**0.70**	**0.39**	**0.23**
iv) $O_{ad} + H2O_{ad} => 2OH_{ad}$	0.35	0.53	0.86	0.57
v) $OO_{ad} + H_{ad} => OOH_{ad}$	0.65	0.57	**0.34**	**0.27**
vi) $OOH_{ad} => O_{ad} + OH_{ad}$	0.03	0.15	**0**	**0**
Rate Det. Step for ORR	0.76	0.70	0.39	0.27

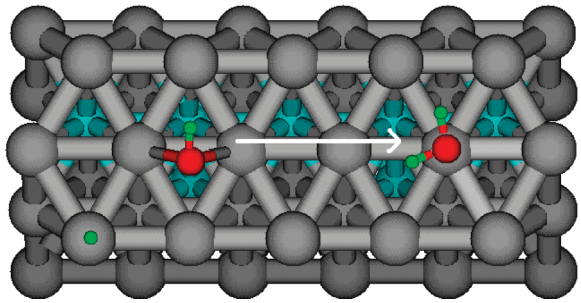

Figure 4. Left: Reaction path for $H_{ad} + OH_{ad} \rightarrow H_2O_{ad}$ on the segregated Pd_3W (111) alloy surface [each point is the quantum mechanics (PBE) energy along the nudged elastic band (NEB) pathway for the vacuum case]. Also shown are energies corrected for solvation by water. Right: Summary of barriers for various reaction steps in the oxygen reduction reaction (ORR) for several catalysts. Numbers are based on quantum mechanics (PBE) in vacuum + solvation in H_2O. Barriers in boldface are important for the rate-determining step either in the O_2 dissociation or OOH association mechanism. Bottom: Picture of a (111) Pd_3W surface before and after the $H_{ad} + OH_{ad} \rightarrow H_2O_{ad}$ reaction.

second most negative d-band center among the Pd alloys is Pd_3W, making it a promising alloy for further study.

Reaction Pathways for ORR. Two general types of pathways have been suggested for ORR,[12,49,50] one involving O_2 dissociation into two chemisorbed O_{ad} and another involving association of O_2 with H to form OOH_{ad}.

O_2 Dissociation Mechanism 1. This proceeds via an initial O_2 dissociation, $O_{2ad} \rightarrow 2O_{ad}$, followed by OH formation by reaction with H (ii: $H + O_{ad} \rightarrow OH_{ad}$) or water (iv: $H_2O + O_{ad} \rightarrow 2OH_{ad}$) and finally H_2O formation, $H + OH_{ad} \rightarrow H_2O_{ad}$.

$$O_2 \underset{i}{\rightarrow} 2O \xrightarrow[ii]{2H} 2OH \xrightarrow[iii]{2H} 2H_2O \qquad (1)$$

OOH Association Mechanism 2. This starts with activation of the O_{2ad} by H to form OOH_{ad}, $H + O_{2ad} \rightarrow OOH_{ad}$, followed by O−O bond cleavage, $OOH_{ad} \rightarrow O_{ad} + OH_{ad}$, and then formation of H_2O from OH by adding H.

$$O_2 \xrightarrow[v]{H} OOH \underset{vi}{\rightarrow} O + OH \xrightarrow[ii]{H} 2OH \xrightarrow[iii]{2H} 2H_2O \qquad (2)$$

Theoretical models have suggested that the O_2 dissociation mechanisms have higher critical barriers making the OOH association mechanism favorable.[50,51] In contrast, experiments have shown that O_2 dissociates quite readily in water environments suggesting the barrier is lower than previous calculations.[52] Thus, there is no consensus on the exact mechanism of ORR, justifying additional studies.

The barriers for various ORR reactions have previously been calculated in various ways including fuel cell operating potentials.[49−51,53] There is no consensus on a method to calculate barriers of reactions of H_3O^+ with adsorbed ORR species. In a pioneering paper, Norskov and co-workers[50] computed the energetics but not the barriers of reactions of hydronium with ORR species. Another study[51] estimated just the barrier of $OO_{ad} + H_3O^+ \rightarrow H_2O + OOH_{ad}$ in water, which was referenced to the electron of H_2 in the fuel cell anode, but no other ORR barriers. In another approach, Kasai et al.[54] computed hydronium barriers with reference to vacuum at zero potential and found in this context that these ORR reactions have no barriers. Although each of these approaches has its merit, each involves simplifying assumptions for the reaction pathway involving hydronium.

Instead, we assume that the H is adsorbed on the Pt surface to compute zero potential barriers. This method has been used in several previous works.[12,27] For all reactions we included solvent effects implicitly to account for the effects of water. These barriers provide insights into the differences in the reaction barriers for various metal and alloys, providing benchmarks for predicting which alloys/metals are best.

These various barriers are shown in Figure 4 for Pt, Pt_3Co, Pd, and Pd_3W.

Implications for ORR. Figure 4 shows dramatic differences between Pt, Pt_3Co, Pd, and Pd_3W in terms of the reaction barriers for the various fundamental steps. For example, the direct OH formation has a low barrier for Pd and Pd_3W (0.41 and 0.26 eV), whereas this barrier is high for Pt_3Co and Pt (0.62 and 1.23 eV). However, for Pt and Pt_3Co the alternative mechanism of OOH formation provides a low barrier of 0.34 and 0.27 eV, respectively.

Also, the H_2O formation barrier, $H_{ad} + OH_{ad} \rightarrow H_2O$, is slightly lower for Pd_3W (0.70 eV) than for pure Pd (0.76 eV).

Since this is the rate-determining step for these cases, the Pd_3W catalysis should be better than that for pure Pd.

Considering that OH is formed by H_{ad} adding to O_{ad} would make this relatively favorable for Pd and Pd_3W (0.41 and 0.26 eV, respectively) but very unfavorable for Pt and Pt_3Co (1.23 and 0.62 eV, respectively). However, in a PEMFC, the OH formation might result by protonation of O_{ad} by solvent H_3O^+.

Thus, we consider that the rate-determining step for ORR on Pt is adding H_{ad} to OH_{ad} to form H_2O_{ad}, with a barrier of 0.39 eV for Pt and 0.23 eV for Pt_3Co. Note that this barrier is 0.76 eV for Pd, significantly higher than that for pure Pt, 0.39 eV. However, for the Pd_3W alloy this barrier is 0.70 eV, an improvement over the barrier of 0.76 eV for pure Pd.

Comparison to Experiment. Until completion of these studies, we were unaware of any previous studies on Pd−W catalysts for fuel cells. Indeed based on our results Debbie Myers of Argonne National Laboratories in December 2008 initiated a series of experiments to validate our predictions.

However, upon completion of our manuscript, an experimental paper was published,[4] showing that alloying of Pd with W enhances the catalytic activity for ORR compared to pure Pd. These experimental studies used nanoparticles with the composition $Pd_{95}W_5$ and found that the maximum activity for the ORR is nearly as good as the activity of Pt. Our study for the infinite slab suggests that the best composition would be Pd_3W.[55,56] (There is a report on the Pd−W phase diagram characterizing the Pd_3W phase as hexagonal.[44] This seems surprising since Pd is fcc cubic, while W is bcc cubic. Also experimental results on Pd−W alloys find that $Pd_{0.6}W_{0.4}$ and $Pd_{3.2}W_{0.8}$ are both fcc, while $Pd_{0.046}W_{0.954}$ is bcc.[55,56]) A difference here is that the experiment deals with carbon-supported nanoparticles having the $Pd_{100-x}W_x$ ($0 \le x \le 30$) face centered cubic solid solutions, whereas our calculations were carried out for the Pd_3W (111) surface assuming two-dimensional infinite slabs.

No electrochemical data were presented or discussed in ref 4 for $Pd_{70}W_{30}$ (which is close in composition to Pd_3W). Clearly further investigations of these alloys, including Pd_3W, is in order, particularly its catalytic activity for ORR. These computational results on Pd_3W suggest that Pd_3Mo should also be segregated and effective for ORR. Indeed experiments indicate that Pd−Mo is also a good ORR catalyst.[57]

Summary and Conclusion

We examined 80 binary alloys with composition Y_3X to find 12 systems with a strong driving force to segregate with the noble metal Y at the surface and the more electropositive metal X preferring the second layer, which we expect to provide good ORR performance simultaneous with stability under oxidation conditions. We compared our segregation results with experimental LEED results and find that they agree well. We further compared the second layer enrichment of 3d base atoms in Pt alloys and found that some alloys have a higher energy penalty to be enriched in the second layer, leading to negative segregation energy. We find that the second layer enrichment of the 3d atom is such that Pt_3Ni (high) > Pt_3Co (high) > Pt_3Fe (moderate) > Pt_3Ti (low), agreeing well with experimental results. We also examined surface d-band centers of the these alloys with 100% Pt first layer and 50% Pt second layer and found Pd_3Ta and Pd_3W to be non-Pt alloys with d-band centers closest to Pt. From this set we examined the ORR performance on the Pd_3W system, which we considered the best candidate. Indeed we predict much better performance than for pure Pd, perhaps close to that of pure Pt. Since the cost of this material[1] would be ca. $^1/_6$ that of pure Pt, we suggest experimental examination of catalysts with compositions near that of Pd_3W. Moreover such systems should be more stable under oxidizing conditions of the fuel cell. We found a number of good candidates with alloys of W, Ta, V, and Nb particularly favorable. We chose to focus first on Pd_3W since it is a known intermetallic compound and has a d-band center close to Pt.

We examined the various reaction steps for ORR, with the hope that the rate for Pd_3W would be substantially better than that for Pd, just as Pt_3Co is better than Pt. Indeed we found Pd_3W to have substantially lower barriers than Pd, nearly as good as Pt and Pt_3Co. If Pd_3W turns out to be less sensitive to leaching under oxidative conditions as suggested from our calculations, its lower coast by a factor of 6 could make it a practical alternative to Pt for PEM fuel cells.

The rate-determining step for both Pd and Pd_3W is the water formation, but the corresponding barrier is lower for the Pd_3W alloy, 0.70 eV, compared to that for pure Pd, 0.76 eV.

Due to the favorable segregation energy and overall energetics which is similar to that of Pt, Pd_3W can be considered as a promising candidate for further theoretical and experimental investigations of its catalytic properties. According to our computational data, Pd_3Ta, Pd_3V, and Pd_3Nb are other promising candidates for further review.

Acknowledgment. This work was supported by the U.S. Department of Energy under grant DE-AC02-06CH11357. The facilities of the Materials and Process Simulation Center (MSC) used in this study were established with grants from DURIP-ONR, DURIP-ARO, and NSF-MRI. Additional support for fuel cell research in the MSC is provided by Ford Scientific Research Laboratories. We thank Dr. Deborah Meyers, Dr. Gerald Voecks, and Prof. Clemens Heske for useful discussions.

Supporting Information Available: Optimized lattice parameters for various Y_3X metal alloys, segregation energy of 4-, 5-, and 6-layer slabs to verify that the 4-layer slab model is sufficient, and optimized spin of Y_3X alloy surface segregated 4-layer surfaces and bulk structures. This material is available free of charge via the Internet at http://pubs.acs.org.

References and Notes

(1) All Metal Quotes: www.kitco.com/market/.
(2) Kinoshita, K. *Electrochemical Oxygen Technology*; Wiley: New York, 1992.
(3) Fernandez, J. L.; Raghuveer, V.; Manthiram, A.; Bard, A. J. *J. Am. Chem. Soc.* **2005**, *127*, 13100–13101.
(4) Sarkar, A.; Murugan, A. V.; Manthiram, A. *J. Mater. Chem.* **2009**, *19*, 159–165.
(5) Markovic, N. M.; Ross, P. N. *Surf. Sci. Rep.* **2002**, *45*, 121–229.
(6) Stamenkovic, V. R.; Fowler, B.; Mun, B. S.; Wang, G. F.; Ross, P. N.; Lucas, C. A.; Markovic, N. M. *Science* **2007**, *315*, 493–497.
(7) Gauthier, Y. *Surf. Rev. Lett.* **1996**, *3*, 1663–1689.
(8) Deckers, S.; Habraken, F. H. P. M.; Vanderweg, W. F.; Vandergon, A. W. D.; Pluis, B.; Vanderveen, J. F.; Baudoing, R. *Phys. Rev. B* **1990**, *42*, 3253–3259.
(9) Watanabe, M.; Tsurumi, K.; Mizukami, T.; Nakamura, T.; Stonehart, P. *J. Electrochem. Soc.* **1994**, *141*, 2659–2668.
(10) Nilekar, A. U.; Ruban, A. V.; Mavrikakis, M. *Surf. Sci.* **2009**, *603*, 91–96.
(11) Ruban, A. V.; Skriver, H. L.; Norskov, J. K. *Phys. Rev. B* **1999**, *59*, 15990–16000.
(12) Jacob, T.; Goddard, W. A. *ChemPhysChem* **2006**, *7*, 992–1005.
(13) Ma, Y. G.; Balbuena, P. B. *Surf. Sci.* **2008**, *602*, 107–113.
(14) Perdew, J. P.; Burke, K.; Ernzerhof, M. *Phys. Rev. Lett.* **1996**, *77*, 3865–3868.
(15) Schultz, P. SeqQuest, Electronic Structure Code; Sandia National Laboratory, Albuquerque, NM: http://dft.sandia.gov/Quest/.
(16) Feibelman, P. J. *Phys. Rev. B* **1987**, *35*, 2626–2646.
(17) Ceperley, D. M.; Alder, B. J. *Phys. Rev. Lett.* **1980**, *45*, 566–569.
(18) Perdew, J. P.; Zunger, A. *Phys. Rev. B* **1981**, *23*, 5048–5079.

(19) Goddard, W. A. *Phys. Rev.* **1968**, *174*, 659.
(20) Melius, C. F.; Goddard, W. A. *Phys. Rev. A* **1974**, *10*, 1528–1540.
(21) Melius, C. F.; Olafson, B. D.; Goddard, W. A. *Chem. Phys. Lett.* **1974**, *28*, 457–462.
(22) Redondo, A.; Goddard, W. A.; Mcgill, T. C. *Phys. Rev. B* **1977**, *15*, 5038–5048.
(23) Edwards, A. SeqQuest, Post Analysis Code; Sandia National Laboratory, Albuquerque, NM: http://dft.sandia.gov/Quest/SeqQ_Kudos.html.
(24) Kresse, G.; Furthmuller, J. *Phys. Rev. B* **1996**, *54*, 11169–11186.
(25) Baker, N. A.; Sept, D.; Joseph, S.; Holst, M. J.; McCammon, J. A. *Proc. Natl. Acad. Sci. U.S.A.* **2001**, *98*, 10037–10041.
(26) Holst, M. J.; Saied, F. *J. Comput. Chem.* **1995**, *16*, 337–364.
(27) Sha, Y.; Yu, T. H.; Merinov, B. V.; Goddard, W. A. *J. Phys. Chem. Lett.* **2010**, *1*, 856–861.
(28) Lesiak, B.; Bilinski, A.; Jozwik, A. *Surf. Interface Anal.* **2005**, *37*, 1143–1150.
(29) Derry, G. N.; Wan, R. *Surf. Sci.* **2004**, *566*, 862–868.
(30) Stamenkovic, V. R.; Mun, B. S.; Arenz, M.; Mayrhofer, K. J. J.; Lucas, C. A.; Wang, G. F.; Ross, P. N.; Markovic, N. M. *Nat. Mater.* **2007**, *6*, 241–247.
(31) Stamenkovic, V. R.; Mun, B. S.; Mayrhofer, K. J. J.; Ross, P. N.; Markovic, N. M. *J. Am. Chem. Soc.* **2006**, *128*, 8813–8819.
(32) Creemers, C.; Deurinck, P. *Surf. Interface Anal.* **1997**, *25*, 177–190.
(33) Gauthier, Y.; Senhaji, A.; Legrand, B.; Treglia, G.; Becker, C.; Wandelt, K. *Surf. Sci.* **2003**, *527*, 71–79.
(34) Hornstrom, S. E.; Johansson, L. I. *Appl. Surf. Sci.* **1986**, *27*, 235–246.
(35) Gasteiger, H. A.; Ross, P. N.; Cairns, E. J. *Surf. Sci.* **1993**, *293*, 67–80.
(36) Tsong, T. T.; Ren, D. M.; Ahmad, M. *Phys. Rev. B* **1988**, *38*, 7428–7435.
(37) Grgur, B. N.; Markovic, N. M.; Ross, P. N. *J. Phys. Chem. B* **1998**, *102*, 2494–2501.
(38) Brown, D.; Quinn, P. D.; Woodruff, D. P.; Noakes, T. C. Q.; Bailey, P. *Surf. Sci.* **2002**, *497*, 1–12.
(39) Stamenkovic, V. R.; Schmidt, T. J.; Ross, P. N.; Markovic, N. M. *J. Phys. Chem. B* **2002**, *106*, 11970–11979.
(40) Anton, R.; Eggers, H.; Veletas, J. *Thin Solid Films* **1993**, *226*, 39–47.
(41) Wouda, P. T.; Schmid, M.; Nieuwenhuys, B. E.; Varga, P. *Surf. Sci.* **1998**, *417*, 292–300.
(42) Hornstrom, S. E.; Johansson, L. I.; Flodstrom, A. *Appl. Surf. Sci.* **1986**, *26*, 27–41.
(43) Tsong, T. T.; Ng, Y. S.; Mclane, S. B. *J. Chem. Phys.* **1980**, *73*, 1464–1468.
(44) Alloy Phase Diagrams Center: www.asminternational.org/AsmEnterprise/APD/.
(45) Naidu, S. V. N.; Rao, P. R. *Alloy Phase Diagrams* **1990**, *16*, 67.
(46) Darby, J. B.; Downey, J. W.; Norton, L. J. *Trans. Metall. Soc. AIME* **1963**, *227*, 1028.
(47) Chen, W. H.; Paul, J. A. K.; Barbieri, A.; Vanhove, M. A.; Cameron, S.; Dwyer, D. J. *J. Phys.: Condens. Matter* **1993**, *5*, 4585–4594.
(48) Hammer, B.; Norskov, J. K. *Surf. Sci.* **1995**, *343*, 211–220.
(49) Kitchin, J. R.; Norskov, J. K.; Barteau, M. A.; Chen, J. G. *J. Chem. Phys.* **2004**, *120*, 10240–10246.
(50) Anderson, A. B.; Albu, T. V. *J. Electrochem. Soc.* **2000**, *147*, 4229–4238.
(51) Norskov, J. K.; Rossmeisl, J.; Logadottir, A.; Lindqvist, L.; Kitchin, J. R.; Bligaard, T.; Jonsson, H. *J. Phys. Chem. B* **2004**, *108*, 17886–17892.
(52) Janik, M. J.; Taylor, C. D.; Neurock, M. *J. Electrochem. Soc.* **2009**, *156*, B126–B135.
(53) Ogasawara, H.; Naslund, L. A.; Macnaughton, J. B.; Anniyev, T. A. N. *ECS Trans.* **2008**, *16*, 1385.
(54) Filhol, J. S.; Neurock, M. *Angew. Chem., Int. Ed.* **2006**, *45*, 402–406.
(55) Son, D. N.; Nakanishi, H.; David, M. Y.; Kasai, H. *J. Phys. Soc. Jpn.* **2009**, *78*.
(56) Luo, H. L. *J. Less-Common Met* **1968**, *15*, 299.
(57) Goetz, W. K.; Brophy, J. H. *J. Less-Common Met.* **1964**, *6*, 345–353.
(58) Sarkar, A.; Murugan, A. V.; Manthiram, A. *J. Phys. Chem. C* **2008**, *112*, 12037–12043.

JP1024735